Electronic Supplementary Information (**ESI†**).

Probing Battery Chemistry with Liquid Cell Electron Energy Loss Spectroscopy

Raymond R. Unocic,[a*] Loïc Baggetto,[b] Gabriel M. Veith,[b] Jeffery A. Aguiar,[c]
Kinga A. Unocic,[b] Robert L. Sacci,[b] Nancy J. Dudney,[b] Karren L. More[a]

[a] Center for Nanophase Materials Science, Oak Ridge National Laboratory, Oak Ridge, TN, 37831
[b] Materials Science and Technology Division, Oak Ridge National Laboratory, Oak Ridge, TN 37831
[c] Microscopy and Imaging Group, National Renewable Energy Laboratory, Golden, CO 80401

Thin film deposition

Radio frequency magnetron sputtering was used to deposit thin films of $LiMn_2O_4$ and $Li_4Ti_5O_{12}$ directly onto the silicon microchip platforms for *in situ* liquid EELS measurements. The $Li_4Ti_5O_{12}$ sputtering target was prepared by high temperature solid-state reaction and the compositions were obtained by mixing appropriate quantities of Li_2CO_3 and TiO_2. A commercial powder from Cerac was sintered to prepare the $LiMn_2O_4$ target. Sputtering was performed at 80W, with a 5 mTorr Ar pressure using 57 sccm Ar and a target-substrate distance of 5 cm. The films initially are amorphous and therefore required a post-deposition annealing heat treatment at 450º C for 20 min using 10º C min^{-1} heating and cooling rates.

Liquid cell microscopy

A Hummingbird Scientific liquid flow cell *in situ* TEM system was used in these experiments. RF magnetron sputtering was used to deposit the thin film electrode material only on one of the blank silicon microchip devices. (**Figure S1**)

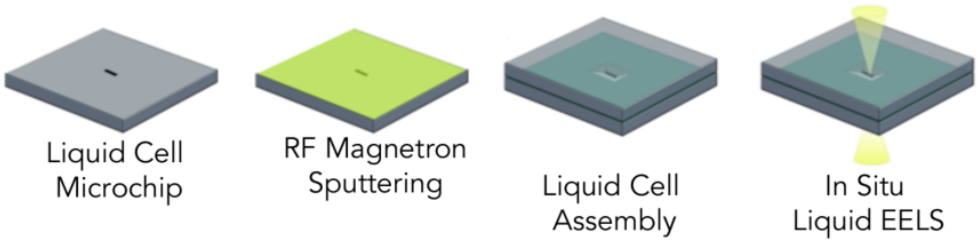

Figure S1. Illustration of RF sputtered thin films on the liquid cell silicon microchip devices and assembly of the microchips for in situ liquid EELS measurements.

Crystal structure determination through selected area electron diffraction

The crystal structure of the thin films were determined through selected area electron diffraction (SAED). **Table SI** shows the experimental measured d-spacings from the SAED ring patterns corresponding to $LiMn_2O_4$ and $Li_4Ti_5O_{12}$ in **Figure 1a,c**.

Table SI. Selected area electron diffraction pattern measurements.

Ring #	(hkl)	$LiMn_2O_4$ Measured d-spacing (nm)	$LiMn_2O_4$ d_{hkl} JCPDS 035-0782	$Li_4Ti_5O_{12}$ Measured d-spacing (nm)	$Li_4Ti_5O_{12}$ d_{hkl} JCPDS 49-0207
1	111	0.473	0.476	0.489	0.483
2	311	0.246	0.249	0.259	0.252
3	400	0.203	0.206	0.211	0.209
4	333	0.155	0.159	0.166	0.161
5	440	0.142	0.146	0.150	0.148

Liquid Cell Assembly

To form the liquid cell, the silicon microchips were stacked upon one another then inserted into the tip of the *in situ* liquid cell TEM holder. To place the DMC solvent between the microchips one of two methods were used. In the first method, the solvent was dispensed onto the lower microchip device using a pipette. Due to the fast evaporation rate of DMC, the microchip was quickly covered with the second microchip then sealed in the in situ TEM holder. In the second method, the DMC was delivered to microchips that were already sealed within the tip of the in situ TEM holder using a microfluidic delivery system. In the experimental EELS measurements presented in the main body of the manuscript no spacer microchip was used and therefore the first method of dispensing DMC was used. To examine the influence of fluid layer thickness, a 500 nm spacer microchip was used and the DMC was delivered to the microchips using the second method. All EELS measurements were performed at the corner of the silicon nitride membrane in order to minimize membrane bowing and concomitant fluid layer thickness increase.

A bright-field TEM image showing the corner location of the $Li_4Ti_5O_{12}$ within the liquid cell assembly is shown in **Figure S2a**. Note: The speckled contrast on the silicon nitride membrane results from the sputtered nanocrystalline $Li_4Ti_5O_{12}$. To confirm that the DMC solvent was present in each of the liquid EELS measurements reported in this manuscript, the electron dose was increased to induce radiolysis. **Figure S2b** shows bubble formation when DMC is present in the cell, which again was used as an indicator the DMC did not evaporate and was

present in the cell. Note the contrast from the nanocrystalline $Li_4Ti_5O_{12}$ in the background. The DMC liquid layer thickness effect is shown in the low-loss EEL spectra in **Figure S3** where it can be seen that multiple inelastic scattering makes causes an increase in the plasmon peak. The increase in the plasmon peak height relative to the zero loss peak further strengthens there is liquid inside the in situ cell.

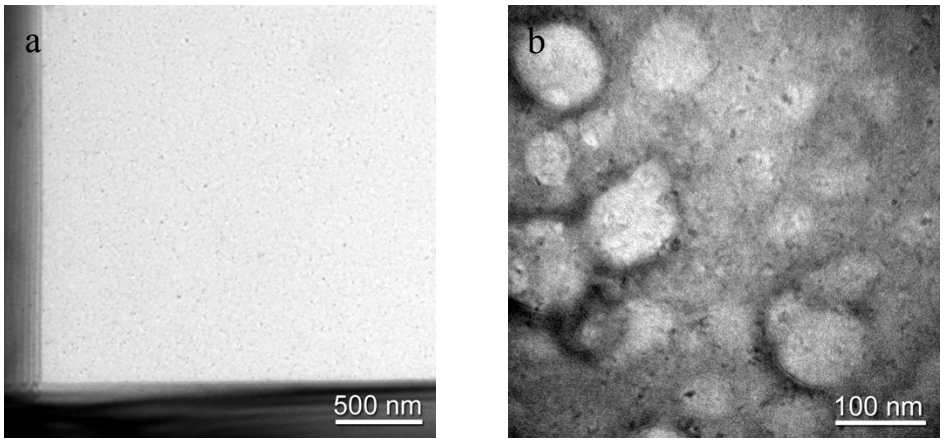

Figure S2. Bright-field TEM images of $Li_4Ti_5O_{12}$ deposited onto one of the silicon nitride membranes and sandwiched between two silicon nitride membranes showing a) the location for EELS measurements (imaged dry) and b) bubble formation in the liquid cell when electron dose is increased to confirm the presence of DMC in the liquid cell.

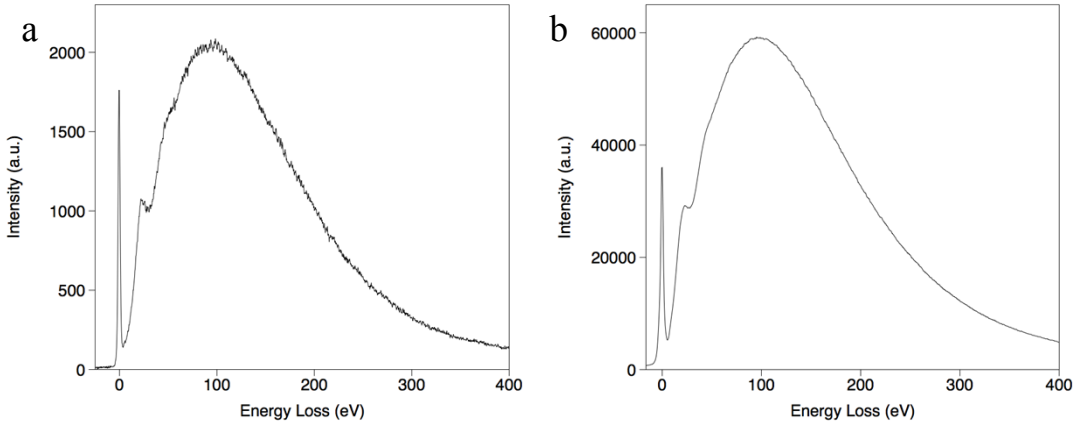

Figure S3. Low loss EEL spectra from a) $LiMn_2O_4$ and b) $Li_4Ti_5O_{12}$ using a 500 nm spacer microchip was used to show the influence of fluid layer thickness on plural scattering. It is clear from these spectra that DMC is present in the liquid cell. (Compare to the relative intensities with the data shown in Figure 2).

Determination of Liquid Layer Thickness

Measurement of the inelastic mean free path attained from the low loss EEL spectra was used to determine the thickness of the liquid from the atomic number formula approximation.[1-2] In this method, liquid cell thickness is determined by first estimating an effective atomic number (Z_{eff}) , which is defined as follows:

$$Z_{eff} = \frac{\sum f_n Z_n^{1.3}}{\sum f_n Z_n^{0.3}} \qquad (1)$$

where f_n is the atomic fraction of element (n) and Z_n is the atomic number of element (n). Given the stoichiometry of the materials within the liquid cell: $LiMn_2O_4$, $Li_4Ti_5O_{12}$, $C_3H_6O_3$ (DMC), and Si_3N_4 (assuming stoichiometric Si_3N_4 for the membranes). Z_{eff} for $LiMn_2O_4$ (dry) and $LiMn_2O_4$ (with DMC) was determined to be 13.84 and 9.63, respectively. Likewise Z_{eff} for $Li_4Ti_5O_{12}$ (dry) and $Li_4Ti_5O_{12\ 4}$ (with DMC) was determined to be 12.76 and 9.91, respectively. λ_i can then be determined through the following approximation:

$$\lambda_i = \frac{106FE_0}{E_M \ln(2\beta E_0 / E_M)} \qquad (2)$$

where F is the relativistic factor for 300kV (0.51), E_o is the accelerating voltage (300kV), β is the collection semi-angle, and E_M is defined as:

$$E_M = 7.6Z_{eff}^{0.36} \qquad (3)$$

Assuming a small collection semi-angle of 7.6 mrad, **Table SII** summarizes the calculated values of Z_{eff} and λ_i for the $LiMn_2O_4$ and $Li_4Ti_5O_{12}$, with and without DMC. From the experimental measurement of t/λ from the low loss EEL spectra, we then calculate the thickness of the liquid layer when DMC is present within the liquid cell which is approximately 101.05 and 60.5 nm for the measurements with $LiMn_2O_4$ and $Li_4Ti_5O_{12}$, respectively. Further details on liquid EELS

measurements, quantification of liquid layer thickness, and measurement error can be found in the manuscript by Jungjohann et al.[2]

Table SII. Liquid layer thickness measurements from calculated values of Z_{eff}, λ_i, and experimental measurements of t/λ .

	$LiMn_2O_4$ (Dry)	**$LiMn_2O_4$ (w/DMC)**	**$Li_4Ti_5O_{12}$ (Dry)**	**$Li_4Ti_5O_{12}$ (w/DMC)**
Z_{eff}	13.84	9.63	12.76	9.91
λ_i	153.09	170.35	156.80	168.81
t/λ measured)	0.92	1.42	0.82	1.12
t	140.84 nm	241.90 nm	128.58 nm	189.07 nm
t (DMC)		**101.05 nm**		**60.5 nm**

Core-Loss Electron Energy Loss Spectroscopy

Due to plural scattering effects the Li K-edge at 55 eV was not distinguishable in the EELS measurements within the low loss EELS spectra (Refer to Figure 2 in the manuscript and Figure S3 in the ESI). Liquid cell chemistry associated with manganese and titanium was studied using core-loss electron energy loss. Both the manganese and titanium L-edges were obtained, that represent a sampling of the unoccupied partial 3*d* density of states above the Fermi energy. Analyzing the core-loss near edge fine structure associated with these element specific spectra provides a detailed perspective into the ionic or valence state with each of these elements. However, in order to determine this information, a sufficient background model, including the effects of plural scattering, backing radiation and the inherent core-loss ionization profile broadened by the intrinsic lifetimes must be routinely subtracted.[3] Only after routinely subtracting these profiles, did we then perform peak fitting of the residual profiles. Specifically, individual Lorentzian peaks were fit over a set of standards of known valence state separately for manganese and titanium. The manganese and titanium $L_{2,3}$ edge was fit with four peaks to within a 97% or better residual mean square value as shown in **Figure S4**. Based on these fits, calibration curves of individual integrated peak intensities, subtended areas, and their ratios were complied for manganese and titanium and used to catalog against samples within the liquid cell. The uncertainty in the analysis is attributed to fitting the peaks and performing a routine background

subtraction. Based on the literature, this was performed by keeping our standard fitting windows, initial fitting parameters, and model refinements fixed over the course of the experiments and analysis. This includes tuning the energy resolution and zero-loss beam profile to within the same values over the course of several experiments.

Given the liquid cell EELS measurements are taken after the electrons have passed through two silicon nitride windows, the liquid media and the sample the inherent plural scattering associated with the interaction of electrons is significantly altered compared to a dry static experiment. Surprisingly, given the robust quantification routines developed through fitting profiles and peaks these effects where not as significant as one might expect. Signal to noise although degraded was enough over background measuring nearly 10 dB, which is beyond the threshold for EELS quantification.

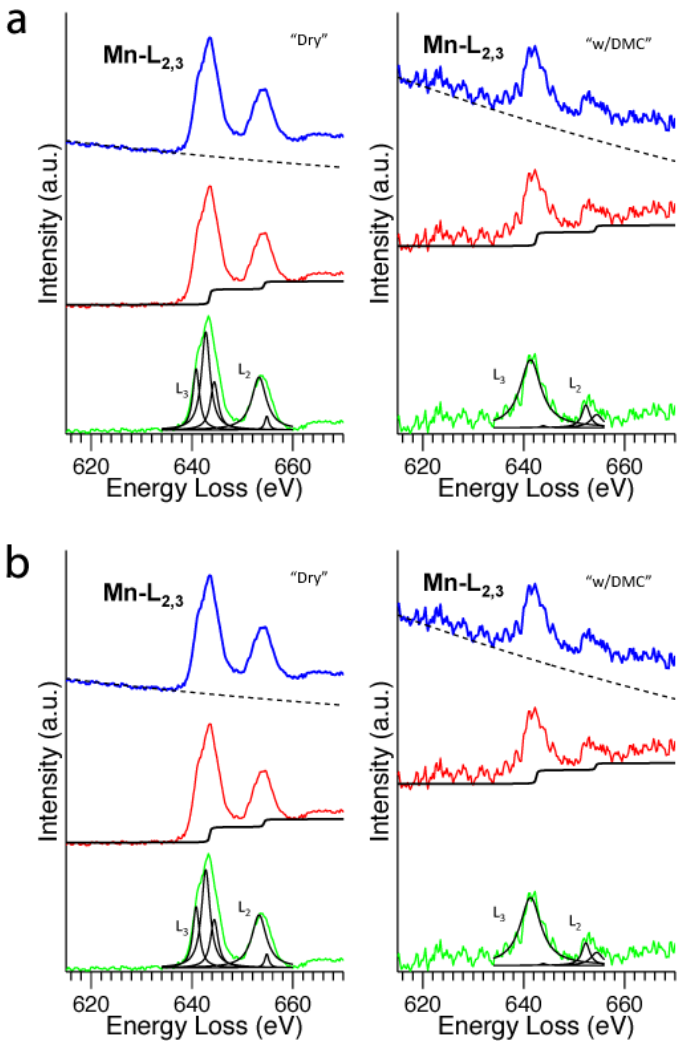

Figure. S4. Core-loss electron energy loss spectra of the a) manganese and b) titanium L-edge were analyzed by minimizing plural scattering by taking a Fourier-log, subtracting a background

model, and fitting four Lorentzian style peaks to the residual near-edge core-loss profile. Shown here is fitting a Mn and Ti L-edges near profile taken within a liquid environment following that procedure with the raw, ionization profile, and individual Lorentzian peaks fitted to the final residual near edge profile. Performing peak fits to our residual near edge EEL spectra then allowed us to systematically catalog the peak intensities, subtended areas, and ratios over a series of known valence state materials containing either titantium or manganese. This data was later used to determine the unknown valence state of our materials using core-loss EEL spectra.

X-ray photoelectron spectroscopy

Surface chemistry of witness electrode samples was probed with a PHI 3056 XPS spectrometer using a Al K source (1486.6 eV). High resolution scans were acquired at 350 W, 23.5 eV constant pass energy, and 0.05 eV energy step, and survey scans were measured at 350 W, 93.9 eV constant pass energy, and 0.5 eV energy step. The energy scale was adjusted by setting the C 1s signal related to adventitious carbon to 284.8 eV.

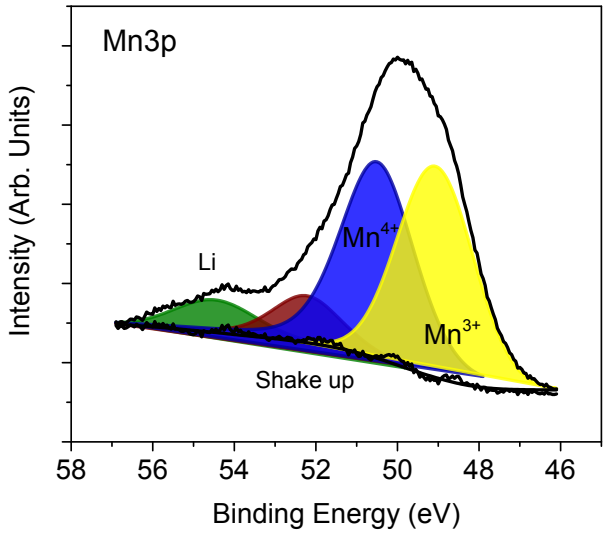

Figure. S5. High resolution X-ray photoelectron spectra (Mn 3p) of the starting $LiMn_2O_4$ thin film material. Assignments are indicated on the figure.

References

1. T. Malis, S.C. Cheng, R.F. Egerton, EELS log-ration technique for specimen-thickness measurement in the TEM, J Electron Microsc. Tech.,8,193-200, 1988.

2. K.L. Jungjohann, J.E. Evans, J.A. Aguiar, I. Arslan, N.D. Browning, Atomic-Scale Imaging and Spectroscopy for In situ Liquid Scanning Transmission Electron Microscopy, Microscopy and Microanalysis, 18, 621-627, 2012.

3. M.O. Krause and J.H Oliver, Natural Widths of Atomic K and L Levels, kα X-Ray lines and Several KLL auger lines, J. Phys. Chem. Ref. Data, Vol. 8, No. 2, 1979.